JMEPEG (2018) 27:2610–2616
https://doi.org/10.1007/s11665-017-3064-1

1059-9495/$19.00

Effect of Reaction Parameters on Morphology and Photoluminescence of Intrinsic and Mn-doped ZnS Microspheres Synthesized by Hydrothermal Method

T. Inakhunbi Chanu, Dhrubajyoti Samanta, Archana Tiwari, and Somenath Chatterjee

(Submitted April 19, 2017; in revised form August 4, 2017; published online November 20, 2017)

Intrinsic and Manganese (Mn)-doped ZnS microspheres have been synthesized by hydrothermal method. Thiourea and amino acid, and L-histidine have been used as sulfur source and capping agent, respectively. The synthesized materials have been characterized using x-ray diffraction, field emission scanning electron microscopy, photoluminescence (PL) and UV–Vis spectroscopy. The above-said characterizations conveyed the information regarding the crystallinity, existence of microspheres, size and optical properties of synthesized ZnS and Mn-doped ZnS samples. Formation of microspheres of intrinsic and Mn-doped ZnS has been observed when the reaction parameters are kept at 150 °C for 4 h, and similarly, the micropores have been noticed when reaction parameters are kept at 150 °C for 8 h. The PL of ZnS microspheres shows multiple defect emissions. The nature of PL for pure ZnS has been regulated based on reaction parameters. Doping of Mn in the ZnS enhances the PL emission. This study reveals the role of reaction parameters and effect of Mn doping on tuning the morphology and emission behavior of ZnS microspheres.

Keywords FESEM, Mn-doped ZnS microsphere, photoluminescence, XRD, ZnS microsphere

1. Introduction

In recent years, significant efforts have been made on tuning the structure of nanomaterials due to its shape- and size-dependent physicochemical properties. ZnS is an important chalcogenide semiconductor material with a band gap energy (E_g) of 3.6 eV. The various forms of ZnS such as quantum dots (QDs), nanobelts, hollow spheres (Ref 1-3) have been reported and have shown applications in various fields. ZnS, having spherical microstructures (including microspheres, micropores and solid spheres), has drawn significant scientific interest and technical importance for their potential application in the field of catalysis, bio-imaging, energy storage and others (Ref 4-6). A number of methods have been employed for the preparation of different microspheres (Ref 7-9). However, proper optimization of synthesis process based on efficiency and cost-effectiveness is still a challenge. Here, we report the recipe of a simple hydrothermal synthesis for the fabrication of large-scale, ZnS and metal-doped ZnS microspheres with tunable size and morphology. The photophysical and photocatalytic efficiency of the ZnS may be enhanced by doping with metal. Recently, Mn-doped ZnS has drawn much attention due to its excellent light-emitting property as luminescent materials. It has been reported that doping with Mn^{2+} ion introduces new energy states within the band gap of host and acts as shallow traps to extend the lifetime of photogenerated charge carriers (Ref 10).

In this work, we demonstrate a simple one-step hydrothermal synthesis process for intrinsic ZnS and Mn-doped ZnS microspheres and the effect of Mn doping on tuning the morphology and emission behavior of synthesized materials. This facile synthetic method allows us to prepare ZnS and Mn-doped ZnS microspheres of controllable size and morphology due to the variation in reaction parameters.

This article is an invited paper selected from presentations at "ICETINN-2017, International Conference on Emerging Trends in Nanoscience and Nanotechnology," held March 16–18, 2017, in Majitar, Sikkim, India, and has been expanded from the original presentation.

T. Inakhunbi Chanu and **Dhrubajyoti Samanta**, Centre for Materials Science and Nanotechnology, Sikkim Manipal Institute of Technology, Sikkim Manipal University, Gangtok, Sikkim, India; **Archana Tiwari**, Department of Physics, Sikkim University, Gangtok, Sikkim, India; and **Somenath Chatterjee**, Centre for Materials Science and Nanotechnology, Sikkim Manipal Institute of Technology, Sikkim Manipal University, Gangtok, Sikkim, India; and Electronics and Communication Engineering Department, Sikkim Manipal Institute of Technology, Sikkim Manipal University, Gangtok, Sikkim, India. Contact e-mail: inakhunbi@gmail.com.

2. Experimental Details

2.1 Chemicals

All chemicals were of analytical grade and used without further purifications. Zinc acetate ($Zn(CH_3COO)_2{\cdot}2H_2O$), manganese acetate ($Mn(CH_3COO)_2{\cdot}4H_2O$) and thiourea ($H_2NCSNH_2$) were purchased from Rankem. L-histidine ($C_6H_9N_3O_2$) was procured from HiMedia. Deionized (DI) water (resistivity 18.5 MΩ-cm) was used for all analyses.

2.2 Instrumentation

X-ray powder diffraction measurements were taken using x-ray diffractometer (PANAlytical Spectris Technologies, Model No. PW 3040/60). Shimadzu 1800 UV–Vis spectrophotometer was used for the measurements of UV–visible absorption spectra of all the samples. PL measurements were taken using

PerkinElmer LS55 fluorescence spectrophotometer. The morphology and composition of the samples were recorded using Zeiss Auriga compact field emission scanning electron microscope (FESEM) equipped with an energy-dispersive x-ray analyzer (EDX). The size of the samples was identified using high-resolution transmission electron microscopy (HRTEM) JEOL 3010 operated at 300 kV.

2.3 Methodology

Intrinsic ZnS microspheres were synthesized following the hydrothermal method reported earlier by our group (Ref 11), with little modification in precursor as well as reaction parameters. $Zn(CH_3COO)_2{\cdot}2H_2O$ and L-histidine were dissolved in DI water and stirred at room temperature for 30 min. Then, thiourea solution was added into the same slowly while stirring. The molar ratio of L-histidine, zinc and sulfur sources was maintained at 1:1:1. The solution was transferred to a 250-mL Teflon-lined stainless steel autoclave system and maintained the final volume at 80 mL. Then, the autoclave was placed inside the preheated muffle furnace at temperature 150 °C for 4 h and then cooled down to room temperature naturally. The solution was centrifuged and washed several times with DI water and methanol to remove the impurities. Finally, the sample was dried at 80 °C for 3 h. Mn-doped ZnS samples were also synthesized by following the same process, except that the $Mn(CH_3COO)_2{\cdot}4H_2O$ was added prior to mixing with thiourea solution. The details of sample notations and reaction parameters are given in Table 1.

3. Results and Discussion

3.1 Structural and Morphological Characterization

Figure 1(a) shows the x-ray diffraction (XRD) patterns of ZnS and Mn-doped ZnS samples synthesized using hydrothermal process with reaction parameters of 150 °C for 4 h, denoted as Z1, MZ1, MZ2, MZ3 and MZ4 (corresponding specifications are mentioned in Table 1). The diffraction peaks observed at 2θ values of 28.6°, 33.1°, 47.6° and 56.4° can be indexed to (111), (200), (220) and (311) planes, respectively, of the cubic zinc blende structure of ZnS, according to JCPDS Card No. 05-0566. The XRD peaks appear to be broadened on increasing the percentage of Mn doping, indicating the influence of Mn in ZnS samples. Inset of Fig. 1(a) depicts the deconvolution for part of XRD peak corresponding to MZ4 sample. The three distinct peaks are observed at 2θ values of 27.5°, 28.6° and 30.9°. The peak at 2θ values of 28.6° corresponds to (111) plane of ZnS, whereas the peaks at 2θ values of 27.5° and 30.9° could be due to the presence of cubic face-centered MnS according to the JCPDS No. 894953. It has been reported that the Zn^{2+} ions may be replaced by Mn^{2+} ions due to the similarity of their ionic radii (Ref 12). This suggests that on increasing the percentage of Mn doping, some of the Zn^{2+} ions could have been replaced by Mn^{2+} ions and MnS-ZnS composites have been formed as confirmed from XRD. The XRD pattern of MZ5 sample is shown in Fig. 1(b). The deconvoluted part (in the inset) shows the presence of peaks at 2θ values of 27.5° and 30.9°, supporting the presence of MnS, which is confirmed from JCPDS No. 894953. The average crystallite sizes of the ZnS and Mn-doped ZnS are calculated using the following Debye–Scherrer equation:

$$D = \frac{k\lambda}{\beta \,\mathrm{Cos}\theta} \qquad \text{(Eq 1)}$$

where $k = 0.9$ is the shape factor, λ is the incident x-ray wavelength of Cu K_α radiation (1.5408 Å), θ is the Bragg diffraction angle, and β is the full width at half maximum (FWHM) of the (111) plane. The crystallite sizes are estimated to be 4.89, 4.82, 4.79, 4.76 and 4.71 nm for Z1, MZ1, MZ2, MZ3 and MZ4, respectively, suggesting the trivial decrease in crystallite size due to the incorporation of Mn.

To determine the presence of L-histidine in the synthesized samples, IR spectrum of Z1 sample is recorded which is shown in Fig. 2. The peaks observed around 3200 cm^{-1} and 1600 cm^{-1} were assigned to the N–H stretching vibrations of the amino group and the C=O stretching of L-histidine (Ref 11, 13), respectively. Therefore, it shows the presence of L-histidine in ZnS samples.

The TEM, FESEM and EDX analysis have been executed to determine the particle size, morphology and elements, respectively. Figure 3(a) and (e) shows the TEM images of Z1 and MZ4 samples. The particles are in the form of microspheres (ranging from 1 to 7 μm) as observed from TEM images. The FESEM images taken at different magnitudes of ZnS sample (i.e., Z1) are shown in Fig. 3(b) and (c). The presence of smooth surface ranging from small to large microspheres can be seen with the appearance of smaller microspheres linked to one another and larger microspheres free. On further verification, the diameter of the microspheres for Z1 sample as obtained from FESEM images is in the range of 1-7 μm. The EDX analysis of the Z1 sample is shown in Fig. 3(d). The presence of two major peaks of Zn and S indicates the purity of the ZnS sample. However, there is a minor trace of carbon, nitrogen and

Table 1 Notations of the hydrothermally synthesized ZnS and Mn-doped ZnS samples

S. no.	Notations	Reaction parameters			Calcination temperature, °C
		Time, h	Temperature, °C	Mn doping, %	
1	Z1	4	150	0	...
2	Z2	8	150	0	...
3	Z3	4	120	0	...
4	Z4	4	150	0	300
5	MZ1	4	150	0.5	...
6	MZ2	4	150	3	...
7	MZ3	4	150	5	...
8	MZ4	4	150	10	...
9	MZ5	8	150	10	...

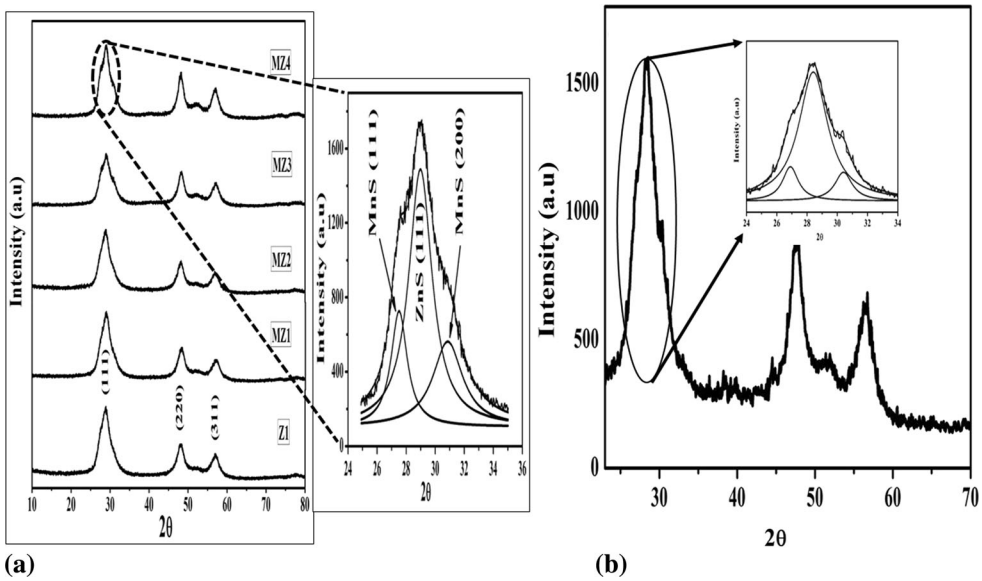

Fig. 1 (a) X-ray diffraction patterns of ZnS and Mn-doped ZnS samples prepared at 150 °C for 4 h (Z1, MZ1, MZ2, MZ3 and MZ4) and inset deconvolution part of the x-ray diffraction patterns of MZ4 sample, (b) x-ray diffraction patterns of MZ5 sample prepared at 150 °C for 8 h and inset showing the deconvolution

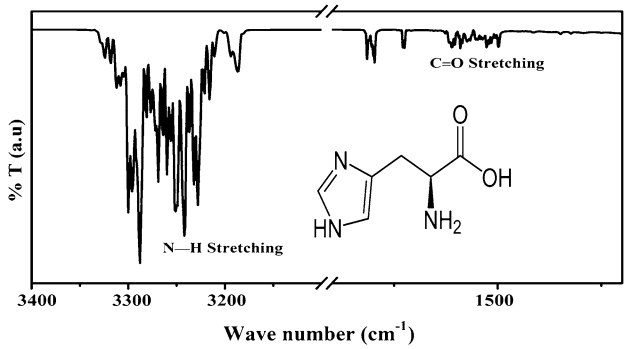

Fig. 2 FTIR spectrum of Z1 sample and inset the molecular structure of L-histidine

oxygen as observed in EDX peaks which might be due to the use of L-histidine as capping agent during the synthesis. The FESEM images for 10% Mn-doped ZnS denoted as MZ4 sample are shown in Fig. 3(f) and (g), which also shows the formation of microspheres with an average size of 1-7 μm. The smaller microspheres appear to be dominant over bigger microspheres in the MZ4 sample. The EDX of the MZ4 sample (Fig. 3h) shows the Mn peak in addition to major Zn and S peaks. This indicates the presence of Mn in ZnS microsphere.

Figure 4(a) and (b) shows the FESEM images of ZnS sample denoted as Z2 which is synthesized at 150 °C for 8 h. It is observed that the particles are in the form of microspheres ranging from smaller microspheres of 1 μm to bigger microspheres of 7 μm. In addition to the microspheres, the presence of micropores is clearly observed in the magnified image (Fig. 4b). It is seen that the bigger particles of 7 μm are dominant over the smaller particles. The EDX analysis shows two major peaks corresponding to Zn and S (Fig. 4c). The FESEM images for 10% Mn-doped ZnS denoted as MZ5 samples are shown in Fig. 4(d) and (e). The presence of micropores in addition to microspheres is also observed in MZ5 sample, suggesting that both Z2 and MZ5 samples have similar morphology, which is quite contrasting from the Z1 and MZ4 samples. This could be due to difference in the reaction parameters: Z1 and MZ4 samples are synthesized at 150 °C for 4 h, whereas Z2 and MZ5 samples are synthesized at 150 °C for 8 h. The EDX of MZ5 sample is shown in Fig. 4(f), showing the presence of Mn peak in addition to Zn and S peaks.

3.2 Optical Properties

The UV–visible absorption spectra of ZnS and Mn-doped ZnS prepared at different reaction parameters are shown in Fig. 5(a). It can be seen from the absorption spectra that the shoulder peak of each spectrum is red-shifted compared to bulk ZnS, indicating the formation of bigger particles. Figure 5(b) displays the Tauc plot of ZnS and Mn-doped ZnS samples. The band gap energy is calculated to be 3.61, 3.56, 3.7 and 3.6 eV for Z1, Z2, MZ4 and MZ5 samples, respectively. The band gap energy of bulk ZnS is 3.6 eV. The lesser band gap energy compared to bulk ZnS suggests the formation of bigger particles, which has also been observed in FESEM images. The band gap energy for Z2 and MZ5 samples is smaller than that for Z1 and MZ4 samples. This suggests that larger particles are dominant over the smaller particles in case of Z2 and MZ5 samples, respectively, which is also supported from FESEM images.

The PL studies for the synthesized ZnS and Mn-doped ZnS were done using excitation wavelength of 300 nm, and the PL emission spectra were measured in the range of 320-580 nm. The baseline correction was done for all PL spectra. The PL spectra of ZnS prepared at different reaction parameters are shown in Fig. 6(a). Multiple defect emission peaks are observed for synthesized ZnS. For samples Z1, Z2 and Z3, emission peaks are observed at 360, 423 and 486 nm, respectively, whereas Z4 sample, which is a calcined sample, shows the additional peaks at 340 nm.

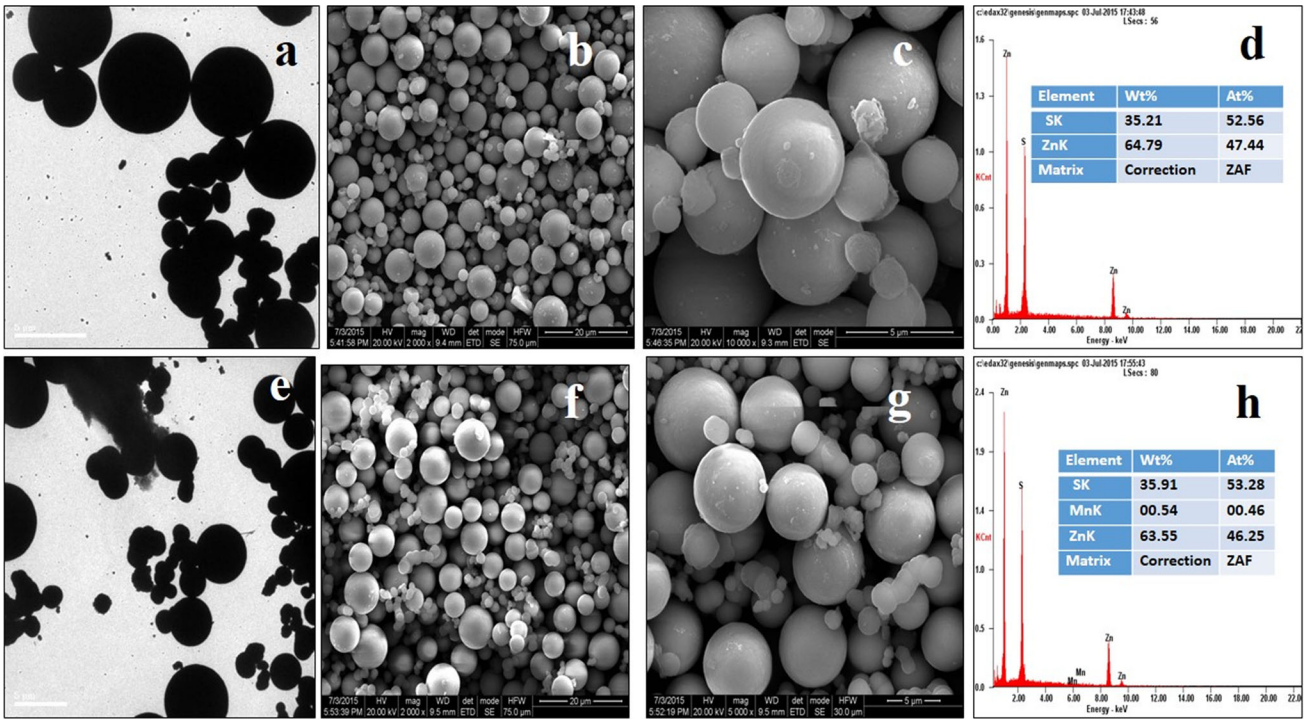

Fig. 3 TEM, FESEM images and EDX of ZnS (Z1) (a to d) and 10% Mn-doped ZnS (MZ4) (e to h) prepared at 150 °C for 4 h

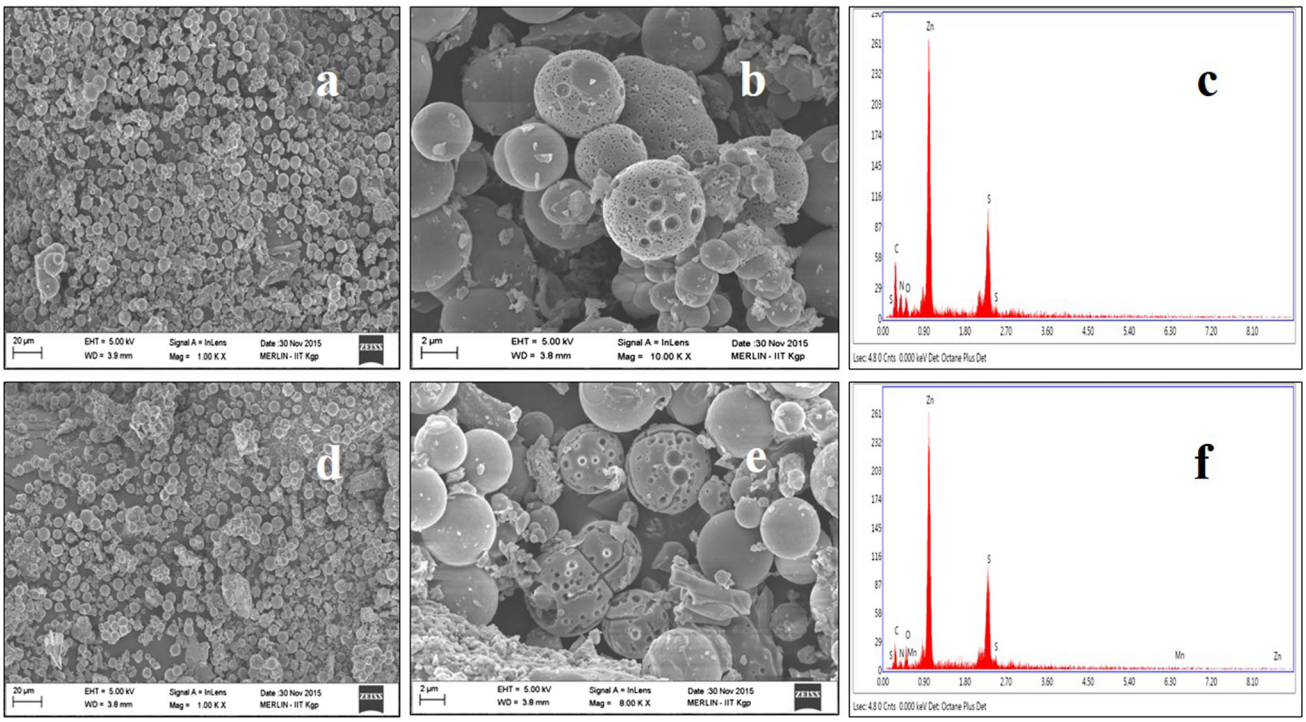

Fig. 4 SEM images and EDX of ZnS (Z2) (a and b) and 10% Mn-doped ZnS (MZ5) (c and d) synthesized at 150 °C for 8 h

Our earlier reported work also showed that the calcined sample distinguishes clearly the band edge emission and defect emission (Ref 11). Accordingly, the peaks are assigned as reported earlier, where the peak at 340 nm is attributed to band edge emission and peaks at 360, 423 and 486 nm are defect emission peaks arising from internal sulfur vacancy and Zn vacancy defect state (Ref 11, 14). For Z2 sample which is prepared at 150 °C for 8 h, the intensity of the defect emission increases as compared to Z1 sample which is prepared at 150 °C for 4 h. And for Z3 sample prepared at 120 °C for 4 h, the intensity decreases as compared to Z1 sample. It suggests that the PL behavior may be tuned just by changing the simple reaction parameters. The nature of emission spectra and efficiency depend on the nature of the nanoparticle surface.

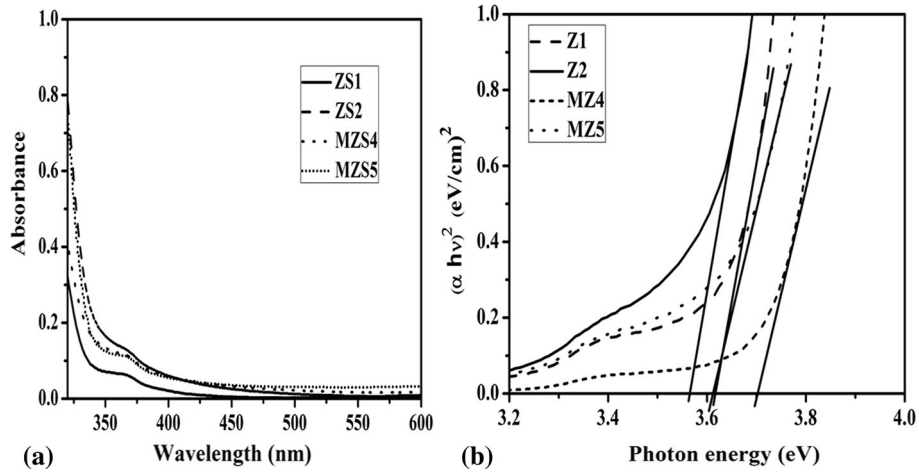

Fig. 5 (a) UV–visible absorption spectra and (b) Taue plot of ZnS and Mn-doped ZnS samples

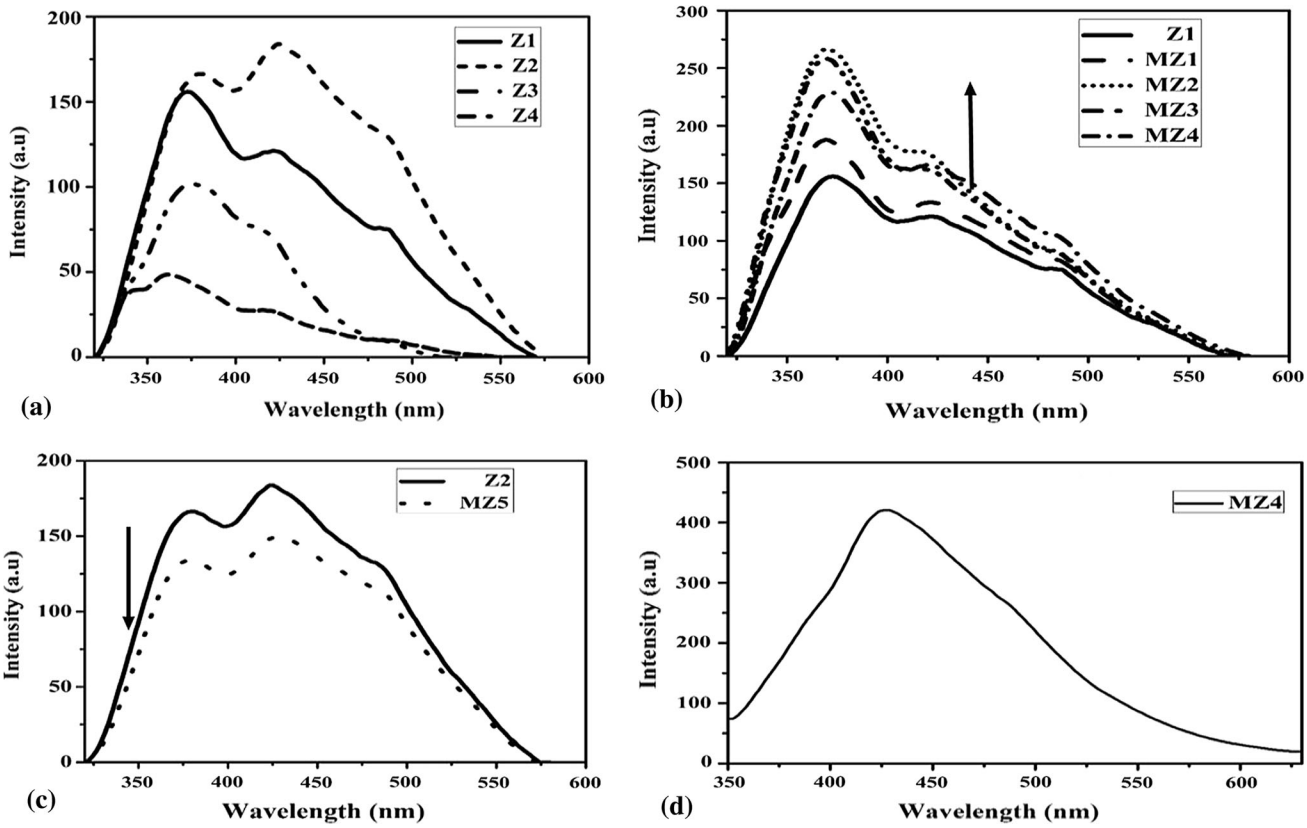

Fig. 6 Photoluminescence spectra of (a) ZnS samples, (b) Mn-doped ZnS denoted as Z1, MZ1, MZ2, MZ3 and MZ4 prepared at 150 °C for 4 h, (c) Mn-doped ZnS denoted as MZ2 and MZ5 prepared at 150 °C for 8 h and (d) MZ4 sample excited at λ_{ex} = 330 nm

Figure 6(b) shows the PL spectra of ZnS and Mn-doped ZnS synthesized at 150 °C for 4 h. The emission intensity of ZnS increases due to increasing the doping percentage of Mn in ZnS sample. For 10% Mn, there is no more increase in emission intensity, suggesting the limiting value for incorporation of Mn in ZnS sample. Figure 6(c) shows the PL spectra of ZnS denoted as Z2 and 10% Mn-doped ZnS denoted as MZ5 samples which are prepared at 150 °C for 8 h. A contrast scenario is observed in Fig. 6(b) and (c). The emission intensity of Z2 sample is higher than that of the MZ5 sample. It has been reported that Mn^{2+} incorporated into the ZnS lattice shows Mn^{2+}-based orange emission due to $^4T_1 - {}^6A_1$ transition within the 3d shell of Mn^{2+}, whereas ZnS with surface-bound Mn^{2+} led to ultraviolet emission (Ref 15-18). In our present study, no peak maxima due to Mn was observed at both ultraviolet and orange emissions. The emission spectrum of MZ4 sample was again measured by exciting the sample at 330 nm and recorded the emission spectrum from 350 to 620 nm, which is shown in Fig. 6(d). No emission peak at 590 nm was observed, suggesting the absence of orange emission arising from Mn. However, the ZnS emission spectra varied on Mn addition. This shows that Mn might disperse in ZnS crystal lattice and act as

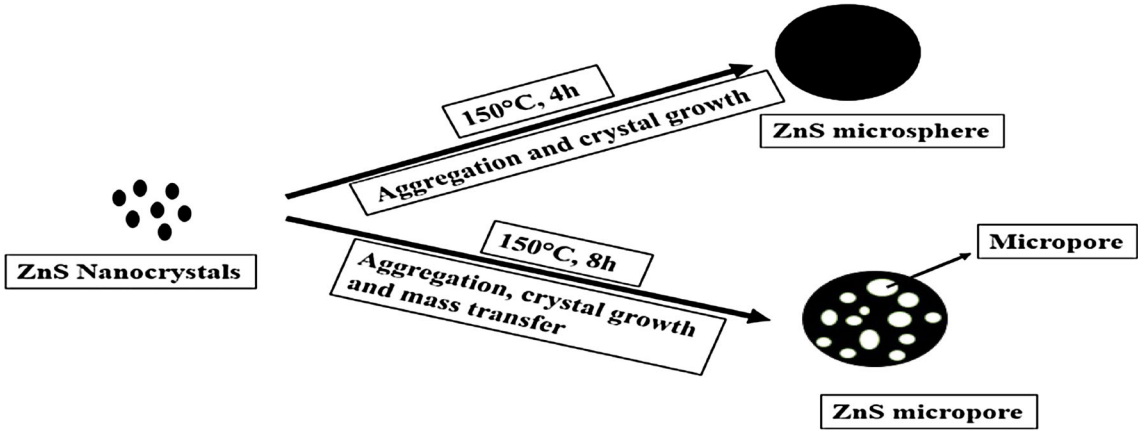

Scheme 1 Mechanism for the formation of ZnS

recombination sites of photogenerated electrons (e^-) and holes (h^+), thereby enhancing the emission spectra of ZnS in case of samples synthesized at 150 °C for 4 h. And for the samples synthesized at 150 °C for 8 h, Mn might act as trap site for generated e^- and h^+ due to the micropore nature of the surface as observed in FESEM images.

3.3 Mechanism for the Formation of Microsphere and Micropore

Initially, the ZnS nanocrystals are formed due to the reaction between the Zn^{2+} ions released from Zn precursor and S^{2-} ions released from thiourea. During the hydrothermal synthesis process, at elevated temperature, thiourea decomposes to give rise to NH_3 and CO_2 in addition to S^{2-} ions (Ref 19). The reaction is shown in Eq 2-4.

$$NH_2CSNH_2 + 2H_2O \rightarrow 2NH_3(g) + 2H_2S(g) + CO_2(g) \quad \text{(Eq 2)}$$

$$H_2S + H_2O \rightarrow HS^- + H_3O^+ \quad \text{(Eq 3)}$$

$$HS^- + H_2O \rightarrow S^{2-} + H_3O^+ \quad \text{(Eq 4)}$$

Since the hydrothermal synthesis process is carried out in airtight closed container autoclave at reaction parameter of 150 °C for 4 h, the production of NH_3 and CO_2 increases which lead to the increase in reaction pressure. Under high reaction pressure condition, the initially formed ZnS nanocrystals tend to form bigger particles due to Ostwald ripening process (Ref 20). The bigger particles are in the form of microsphere to lower the surface energy and surface tension. When the reaction parameters are kept at 150 °C for 8 h, more amounts of NH_3 and CO_2 are produced, which leads to the increase in reaction pressure which will further promote the Ostwald ripening process. The formation of pores may be due to the mass diffusion from the interior smaller size to exterior bigger size as reported by the Huo group (Ref 21). The schematic representation is shown in Scheme 1.

4. Conclusions

In conclusion, ZnS and Mn-doped ZnS microspheres were synthesized by hydrothermal method. The average particle size range is 1-7 µm. Tuning the surface morphology based on reaction parameters, microspheres and micropores of ZnS and Mn-doped ZnS have been synthesized. PL shows the multiple defect emissions. This study demonstrates the role of reaction parameters on tuning the morphology of ZnS and Mn-doped ZnS microspheres. A possible mechanism for the formation of microspheres and as a result micropores in the intrinsic ZnS and Mn-incorporated ZnS samples is discussed here.

Acknowledgments

The authors sincerely acknowledge the Department of Science & Technology (DST), Government of India, for financial support vide reference no. SR/WOS-A/CS-120/2013 under Women Scientist Scheme to carry out this work.

References

1. C. Li, D. Jiang, L. Zhang, J. Xia, and Q. Li, Controlled Synthesis of ZnS Quantum Dots and ZnS Quantum Flakes with Graphene as a Template, *Langmuir*, 2012, **28**, p 9729–9734
2. X. Li, X. Wang, Q. Xionga, and P.C. Eklund, Mechanical Properties of ZnS Nanobelts, *Nano Lett.*, 2005, **5**, p 1982–1986
3. Y. Luo, G. Duan, M. Ye, Y. Zhang, and G. Li, Poly(ethylene glycol)-Mediated Synthesis of Hollow ZnS Microspheres, *J. Phys. Chem. C*, 2008, **112**, p 2349–2352
4. P. Sajan, R.S. Jayasree, S. Agouram, and M.J. Bushiria, Synthesis of Cubic ZnS Microspheres Exhibiting Broad Visible Emission for Bioimaging Applications, *Luminescence*, 2016, **31**, p 544–550
5. C. Wei, C. Cheng, W. Du, J. Ren, M. Li, J. Dong, and K. Liu, Facile Synthesis of Mesoporous Hierarchical ZnS@β-$Ni(OH)_2$ Microspheres for Flexible Solid State Hybrid Supercapacitors, *RSC Adv.*, 2016, **6**, p 101016–101022
6. J. Li, Y. Fu, X. Shi, Z. Xu, and Z. Zhang, Urchin-Like ZnS Microspheres Decorated with Nitrogen-Doped Carbon: A Superior Anode for Lithium and Sodium Storage, *Chem. Eur. J.*, 2017, **23**, p 157–166
7. Q. Yan, A. Wu, H. Yan, Y. Dong, C. Tian, B. Jianga, and H. Fu, Gelatin-Assisted Synthesis of ZnS Hollow Nanospheres: The Microstructure Tuning, Formation Mechanism and Application for Pt-Free Photocatalytic Hydrogen Production, *Cryst. Eng. Comm.*, 2017, **19**, p 461–468
8. L. Yang, J. Han, T. Luo, M. Li, J. Huang, F. Meng, and J. Liu, Morphogenesis and Crystallization of ZnS Microspheres by a Soft Template-Assisted Hydrothermal Route: Synthesis, Growth Mechanism, and Oxygen Sensitivity, *Chem. Asian J.*, 2009, **4**, p 174–180

9. Y. Fang, Z. Xia, F. Yu, J. Sha, Y. Wang, and W. Zhou, Formation Mechanism of Hollow Microspheres Consisting of ZnO Nanosheets, *Cryst. Eng. Comm.*, 2012, **14**, p 8615–8619
10. L. Wang, P. Wang, B. Huang, X. Ma, G. Wang, Y. Dai, X. Zhang, and X. Qina, Synthesis of Mn-Doped ZnS Microspheres with Enhanced Visible Light Photocatalytic Activity, *Appl. Surf. Sci.*, 2017, **391**, p 557–564
11. T.I. Chanu, D. Samanta, A. Tiwari, and S. Chatterjee, Effect of Reaction Parameters on Photoluminescence and Photocatalytic Activity of Zinc Sulfide Nanosphere Synthesized by Hydrothermal Route, *Appl. Surf. Sci.*, 2017, **391**, p 548–556
12. L.M. Gan, B. Liu, C.H. Chew, S.J. Xu, S.J. Chua, G.L. Loy, and G.Q. Xu, Enhanced Photoluminescence and Characterization of Mn-Doped ZnS Nanocrystallites Synthesized in Microemulsion, *Langmuir*, 1997, **13**, p 6427–6431
13. A.B. Ahmed, H. Feki, Y. Abid, H. Boughzala, and C. Minot, Crystal Studies, Vibrational Spectra and Non-linear Optical Properties of L-Histidine Chloride Monohydrate, *Spectrochim. Acta Part A*, 2010, **75**, p 293–298
14. D. Samanta, T.I. Chanu, and S. Chatterjee, Citrus Limetta Juice as Capping Agent in Hydrothermal Synthesis of ZnS Nanosphere for Photocatalytic Activity, *Mater. Res. Bull.*, 2017, **88**, p 85–90
15. A. Goudarzi, G.M. Aval, S.S. Park, M.C. Choi, R. Sahraei, M.H. Ullah, A. Avane, and C.S. Ha, Low-Temperature Growth of Nanocrystalline Mn-Doped ZnS Thin Films Prepared by Chemical Bath Deposition and Optical Properties, *Chem. Mater.*, 2009, **21**, p 2375–2385
16. R.K. Chandrakar, R.N. Baghel, V.K. Chandra, and B.P. Chandra, Synthesis, Characterization and Photoluminescence Studies of Mn Doped ZnS Nanoparticles, *Superlattices Microstruct.*, 2010, **86**, p 256–269
17. H.Y. Chen, S. Maiti, and D.H. Son, Doping Location-Dependent Energy Transfer Dynamics in Mn-Doped CdS/ZnS Nanocrystals, *ACS Nano*, 2012, **6**, p 583–591
18. S. Prasanth, P. Irshad, D.R. Raj, T.V. Vineeshkumar, R. Philip, and C. Sudarsanakumar, Nonlinear Optical Property and Fluorescence Quenching Behavior of PVP Capped ZnS Nanoparticles Co-Doped with Mn^{2+} and Sm^{3+}, *J. Lumin.*, 2015, **166**, p 167–175
19. Y. Zhang, C. Pan, Y. Zhang, and W. He, Self-Template Hydrothermal Synthesis of ZnS Microspheres, *Cryst. Res. Technol.*, 2011, **46**, p 718–722
20. K.P. Ghoderao, S.N. Jamble, J.P. Sawant, and R.B. Kale, Solution Assisted Growth Mechanism and Characterization of ZnS Microspheres, *Mater. Res. Express*, 2017, **4**, p 025026
21. J. Huo, L. Wang, E. Irran, H. Yu, J. Gao, D. Fan, B. Li, J. Wang, W. Ding, A.M. Amin, C. Li, and L. Ma, Hollow Ferrocenyl Coordination Polymer Microspheres with Micropores in Shells Prepared by Ostwald Ripening, *Angew. Chem. Int. Ed.*, 2010, **49**, p 9237–9241